Common Transitions and their Oscillator Strengths

Transition	λ (Å)	J_1	J_2	g_1	g_2	f_{12}
H I $1s-2p$	1215.674	1/2	1/2	2	2	0.1388
	1215.668	1/2	3/2	2	4	0.2775
$^2S-^2P$						0.4163
C IV $2s-2p$	1550.8	1/2	1/2	2	2	0.0951
	1548.2	1/2	3/2	2	4	0.191
$^2S-^2P$						0.286
N V $2s-2p$	1242.8	1/2	1/2	2	2	0.078
	1238.8	1/2	3/2	2	4	0.157
$^2S-^2P$						0.235
O VI $2s-2p$	1037.6	1/2	1/2	2	2	0.0661
	1031.9	1/2	3/2	2	4	0.133
$^2S-^2P$						0.199
Mg II $3s-3p$	2802.7	1/2	1/2	2	2	0.295
	2795.5	1/2	3/2	2	4	0.592
$^2S-^2P$						0.887
Al III $3s-3p$	1862.8	1/2	1/2	2	2	0.286
	1854.7	1/2	3/2	2	4	0.575
$^2S-^2P$						0.861
Si IV $3s-3p$	1402.8	1/2	1/2	2	2	0.224
	1393.8	1/2	3/2	2	4	0.450
$^2S-^2P$						0.674
C III] $2s^2-2s2p$	1908.7	0	1	1	3	1.867×10^{-7}
	1906.7	0	2	1	5	1.414×10^{-11}
$^1S_0-^3P_1$						1.87×10^{-7}
Si III] $3s^2-3s3p$	1892.0	0	1	1	3	2.69×10^{-5}
	1882.7	0	2	1	5	?
$^1S_0-^3P_1$						2.69×10^{-5}
O IV] $2s^22p-2s2p^2$	1399.8	1/2	1/2	2	2	4.52×10^{-7}
	1397.2	1/2	3/2	2	4	2.64×10^{-8}
	1407.4	3/2	1/2	4	2	2.31×10^{-7}
	1404.8	3/2	3/2	4	4	7.57×10^{-8}
	1401.2	3/2	5/2	4	6	5.45×10^{-7}
$^2P-^4P$						7.27×10^{-7}

$$g(J) = \langle n\,sjm| \frac{\mathbf{J}\cdot(\mathbf{L}+2\mathbf{S})}{J(J+1)} |n\,sjm\rangle$$

$$= 1 + \frac{J(J+1) + S(S+1) - L(L+1)}{2J(J+1)}$$

In summary, the magnetic field lifts the degeneracy of the M_J levels (by destroying the spherical symmetry of the total Hamiltonian), and produces a splitting linear in field strength.

Paschen-Back limit. When the magnetic field strength is turned up sufficiently high, so that the Zeeman energy becomes appreciably larger than the spin-orbit coupling energy, we no longer have **J** as a good quantum number. **L** and **S** individually are decoupled (that is, are good quantum numbers), and the Zeeman energy is just

$$E^{(1)}_{\text{Zeeman}} = E(M_L, M_S) = -\frac{e\hbar}{2mc} B_0(M_L + 2M_S) + AM_LM_S$$

where A is the spin-orbit coupling parameter previously introduced.

We can summarize each of these limiting cases by considering the graph shown in Figure 2.16 for the Zeeman splitting of a ^{2}P term. In the low-field region, the

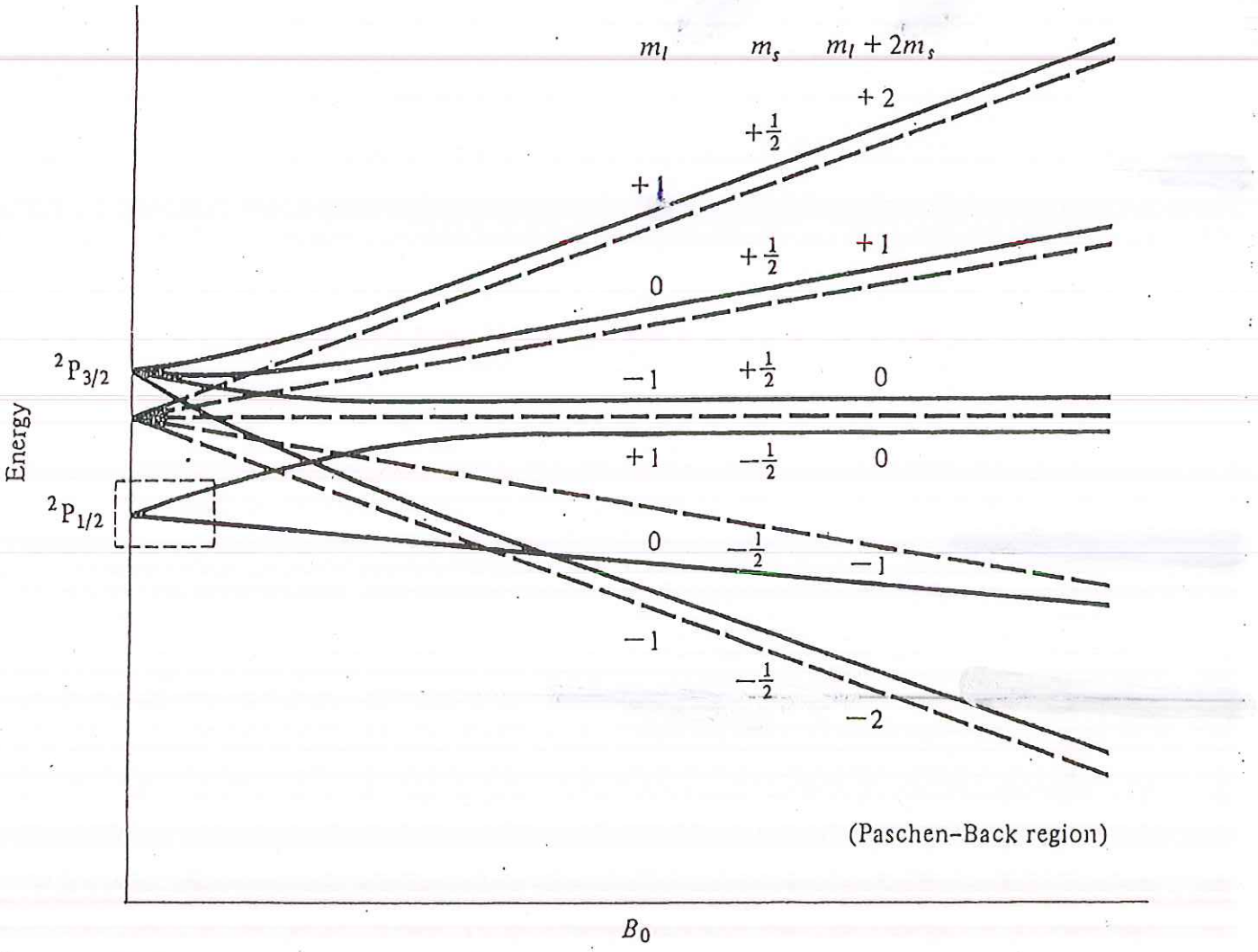

Figure 2.16 Zeeman splitting for a ^{2}P atom. The dashed lines indicate the splittings for the equivalent quintet system in the Paschen-Back limit.

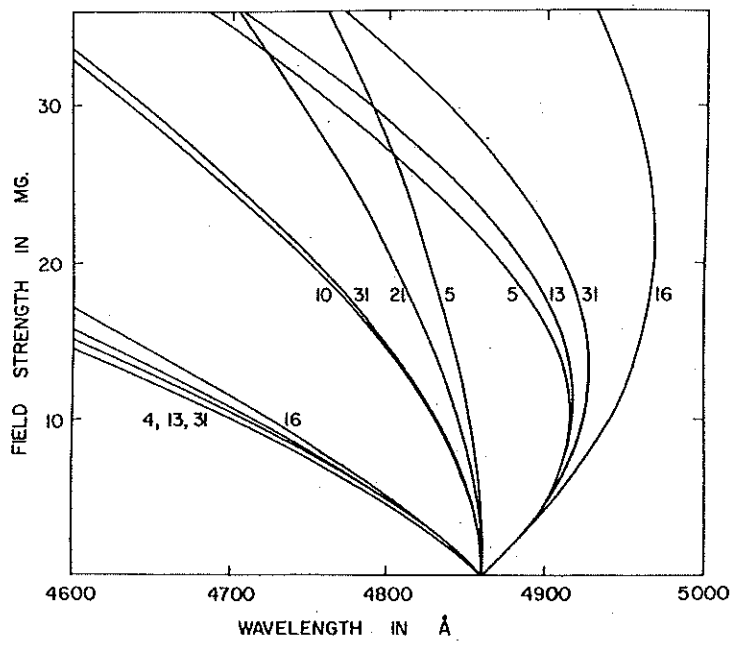

FIG. 2.—The Zeeman splitting of Hβ in fields up to 36 MG. The wavelengths are interpolated from the tables of Kemic (1974) by a fit to the fourth power in *H*. Relative strengths are indicated. A few lines with strength less than 5 have been omitted for clarity.

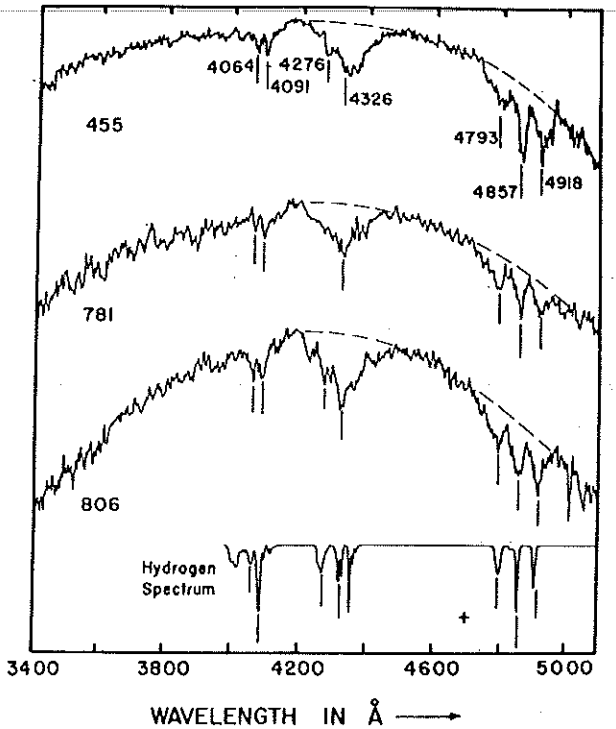

FIG. 3.—*Upper curves*, tracings of three image-tube spectra of GD 90 obtained over a 10 month period in 1972. *Lowest curve*, the absorption spectrum of optically thin hydrogen (Hβ, Hγ, and Hδ only) in a slightly inhomogeneous field of 5×10^6 gauss. The same wavelengths given in the top tracing are marked on each spectrum (Angel *et al.* 1974).

telescope of Steward Observatory are shown in Figure 3. These are taken from the paper identifying GD 90 as a magnetic white dwarf (Angel *et al.* 1974). Underneath is shown the theoretical spectrum of hydrogen, again interpolated for a field uniformly distributed from 4.5 to 5.5 MG from Kemic's tables (1974). The mean value of 5 MG was chosen to give the best fit to the data. The tick marks at wavelengths marked in the top spectrum are repeated at the same wavelength in the other tracings and theoretical spectrum. At Hβ the Zeeman pattern is only weakly affected by the quadratic term, and is seen as a normal Lorentz triplet. Hγ retains a basic triplet structure, though considerably blueshifted, while at Hδ the quadratic term is dominant. All the strong components of this line are below the zero field wavelength (4101 Å). The feature at 4091 Å is identified with the stronger subcomponents of the σ^+ line of Hδ. The identification of the spectroscopic features in GD 90 with magnetically shifted Balmer lines was confirmed by the detection of circular polarization in the blueshifted σ components (σ^-). This result was obtained at Steward Observatory with the 40 element digicon of UCSD and is shown in Figure 4. The σ^- components of Hβ and Hγ are circularly polarized, as expected if the field has a component directed along the line of sight toward the observer. The absence of clear circular polarization of opposite sign at the σ^+ components can be understood if one remembers that their wavelengths are not as sensitive to field changes as are the σ^-, and thus a larger region of the surface with probably positively and negatively directed fields can contribute to the observed σ^+ features.

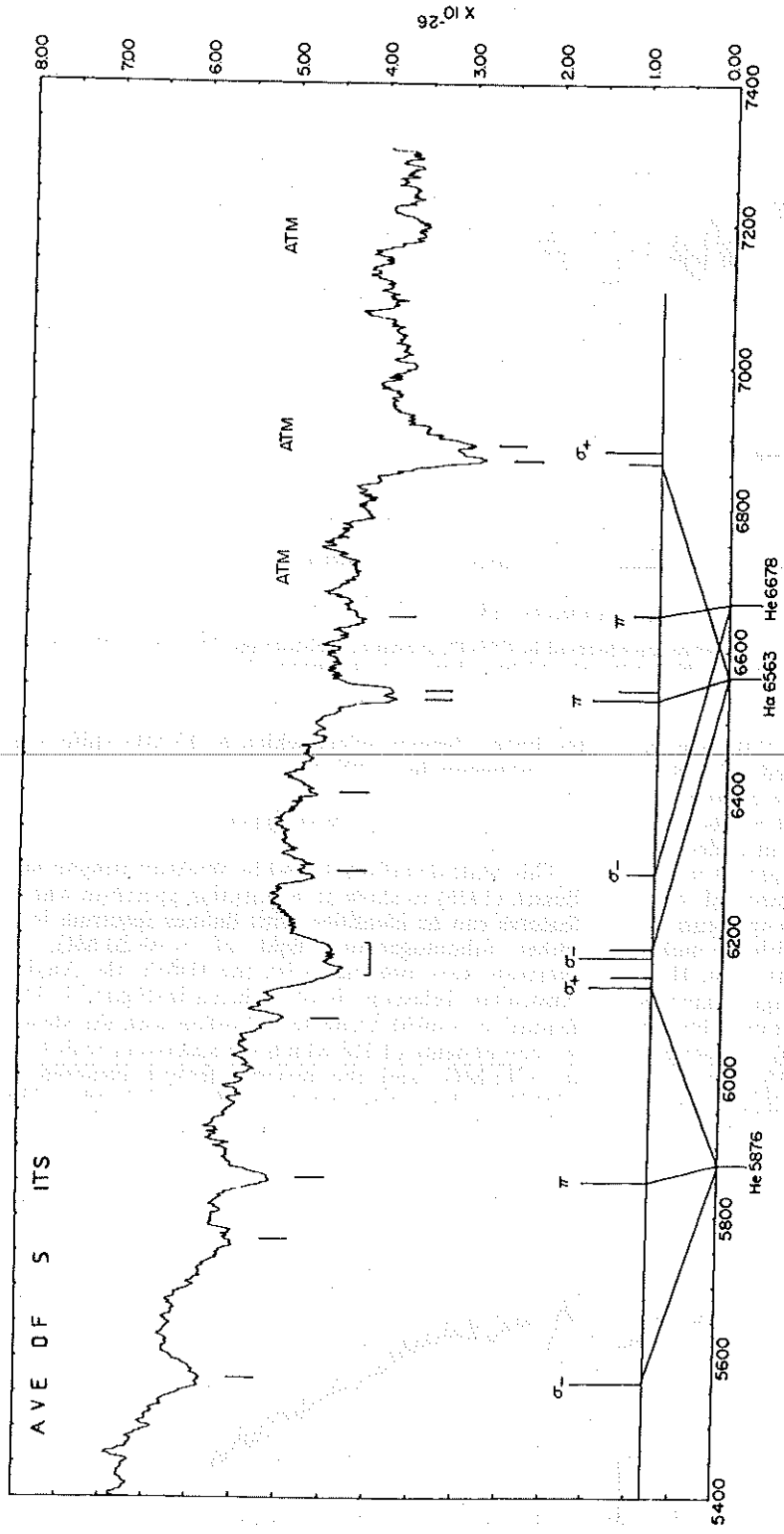

FIG. 8.—A composite red spectrum of Feige 7 which is an average of five scans obtained by Liebert and Spinrad with the ITS at Lick Observatory. Shown below are the Zeeman patterns of Hα and the λ5876 and λ6678 lines of He I, interpolated from Kemic's (1974) tables for a field strength of 18 MG (Liebert *et al.* 1977).

Astron. Astrophys. 211, L31–L34 (1989)

ASTRONOMY AND ASTROPHYSICS

Letter to the Editor

Identification of the emission bands at $\lambda\lambda$6830, 7088

H. M. Schmid

Institute of Astronomy, ETH Zentrum, CH-8092 Zürich, Switzerland

Received November 22, accepted December 20, 1988

Summary. Broad emission bands at 6830 Å and 7088 Å are observed in more than 50 per cent of symbiotic stars. Up to now these features have not been identified. They have only been observed in spectra of symbiotic binaries, which show high excitation emission and M-type absorption. I suggest that the emission features are due to Raman scattering of the OVI resonance doublet $\lambda\lambda$1032, 1038 by neutral hydrogen. In this process the OVI photons are absorbed by hydrogen in its ground state $1s\,^2S$. The absorption leads to an intermediate state from where a photon is emitted, and the hydrogen atom is left in the excited state $2s\,^2S$. According to energy conservation the emitted photons have wavelengths of approximately 6830 Å and 7088 Å. Raman scattering can well explain the observed properties of the emission bands. Physical conditions required for efficient Raman scattering of OVI photons in symbiotic stars will be briefly discussed.

Key words: line identification – symbiotic stars – Raman scattering – emission spectra

1. Introduction

The spectra of symbiotic stars often show a strong, broad emission feature at λ6830. In a subset of stars a weaker but similar band can be observed at about λ7088. An example of these features is shown in Figure 1. The first detection of the λ6830 band was reported by Joy and Swings (1945). They observed that feature in the recurrent nova RS Oph during the 1933 outburst, where it was seen together with coronal emission lines. In later outbursts of RS Oph the λ6830 feature appeared again (e.g. Rosino and Iijima, 1987). Allen (1980) found that approximately half of the symbiotic stars exhibit the λ6830 band. In the same paper he extensively discusses possible identifications. He finds in particular that: (a) The λ6830 band is only observed in the spectra of symbiotic stars. It often ranks among the 10 most intense lines in the optical region, and may reach 5 per cent of the intensity of Hα. The λ7088 band is only seen in objects having strong λ6830 emission. The intensities of the two features correlate, they show an approximate ratio of $I(6830)/I(7088) \approx 4$. (b) The band profiles have a typical width of about 20 Å. The profiles vary strongly from star to star. In a given star there is a similarity between the λ6830 and λ7088 band profiles. (c) The λ6830 band is only observed in high excitation symbiotics showing [NeV] and [FeVII] lines. Thus the λ6830 emission seems to arise from an ion with an ionization potential above 100 eV.

In this letter the emission features λ6830 and λ7088 are identified as Raman scattering of the OVI resonance lines $\lambda\lambda$1032, 1038 by neutral hydrogen. This process can explain all observational properties discussed in Allen (1980), and summarized above.

2. Raman scattering

A basic treatment of the theory for light scattering from a atom can be found in Loudon (1983). Raman scattering of OVI photons by hydrogen is possible, because there exists an excited hydrogen level with an excitation energy below the incident photon energy. Figure 2 shows schematically the scattering path of OVI $\lambda\lambda$1032, 1038 on neutral hydrogen. The incident photon ν_i excites hydrogen from its ground state $1s\,^2S$ to an intermediate

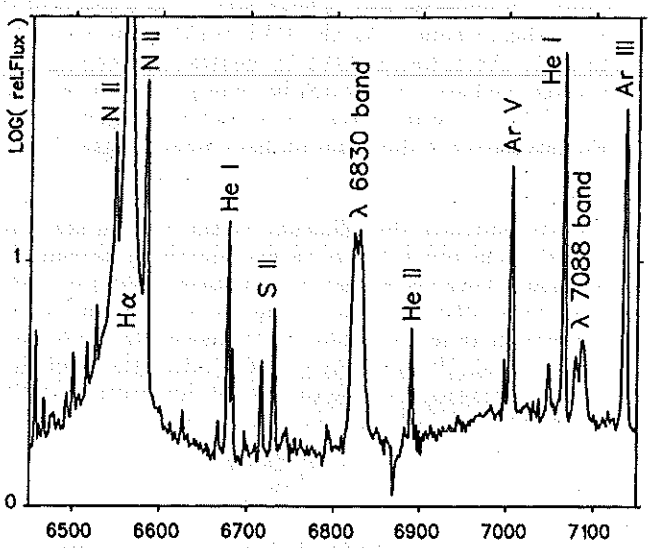

Fig.1. Raman scattered emission bands in the symbiotic star V1016 Cyg. The spectrum was obtained on the 1.93m telescope at the Observatoire de Haute Provence.

Astron. Astrophys. 211, L27–L30 (1989)

ASTRONOMY AND ASTROPHYSICS

Letter to the Editor

Raman scattering as a diagnostic possibility in astrophysics

H. Nussbaumer, H. M. Schmid, and M. Vogel

Institute of Astronomy, ETH Zentrum, CH-8092 Zürich, Switzerland

Received November 29, accepted December 20, 1988

Summary: We show that Raman scattering deserves to be included in the diagnostic tools of the spectroscopy of gaseous nebulae and emission regions of galactic nuclei. We point out that Raman scattering may be the source of some up to now unidentified emission lines. As examples we propose the identification of $\lambda\lambda$1519, 1594 seen in spectra of Seyfert galaxies as Raman scattered Fe XXII and Fe XXIV lines. We show that Raman scattering may act as a line broadening mechanism.

Key words: Raman scattering, Rayleigh scattering, Seyfert galaxies, gaseous nebulae

1. Raman and Rayleigh scattering

Raman scattering describes the absorption of a photon, followed by the immediate re-emission of a photon at different wavelength. Rayleigh scattering describes the absorption of a photon, followed by the immediate re-emission of a photon of the same wavelength. This interaction between photons and atoms has already been described in the classical books on the theory of atomic spectra, e.g. Condon and Shortley (1970, first published 1935), and more detailed treatments can be found in textbooks, e.g. Weissbluth (1978). The two processes differ from ordinary resonant line scattering in that the intermediate state does not correspond to a true bound state of the atom. Figure 1 shows the mechanism of Raman scattering as well as that of Rayleigh scattering which may be regarded as a special case of Raman scattering. A photon of frequency ν_i is absorbed by an atom in an eigenstate $|i>$ with an eigenenergy ϵ_i. The absorption leads to an intermediate state $|q>$ which does not correspond to an eigenstate of the atom, it has an energy

$$\epsilon_q = \epsilon_i + h\nu_i. \tag{1}$$

In a stabilising transition to a true bound state $|f>$ with an eigenenergy ϵ_f the system emits a photon of frequency ν_f. The principle of energy conservation demands that

$$\epsilon_i + h\nu_i = \epsilon_f + h\nu_f. \tag{2}$$

If $\epsilon_f = \epsilon_i$ we talk of Rayleigh scattering, although the term "Rayleigh scattering" is often restricted to cases where $h\nu_i = h\nu_f << \epsilon_m - \epsilon_1$; here we shall employ the term in the wider sense. Thus we designate elastic scattering as Rayleigh scattering and inelastic scattering as Raman scattering.

Isliker et al.(1989) have studied the effect of Rayleigh scattering in atmospheres of red giants within double star systems. At the same time they give formulae for Raman and Rayleigh scattering by hydrogenic ions in a ^{2}S state in terms of oscillator strengths. The formulae are derived by expanding the eigenfunction of the intermediate state $|q>$ in terms of atomic bound state eigenfunctions. The cross-section for Raman scattering by hydrogenic ions as described above is:

$$\sigma^{(\mathrm{Raman})}_{(ns\to n'l')} = \frac{1}{16}\cdot\sigma_e\,\nu_i\nu_f{}^3\left|\sum_m \mathcal{M}^m_{if}\right|^2, \tag{3a}$$

with

$$\mathcal{M}^m_{if} = \sqrt{\frac{(gf)_{fm}}{\nu_{fm}}}\sqrt{\frac{(gf)_{im}}{\nu_{im}}}\,\frac{(\nu_{im}+\nu_{fm})}{(\nu_{im}-\nu_i)(\nu_{fm}+\nu_i)}, \tag{3b}$$

where $|i> = |ns>$ and $|f> = |n'l'>$. σ_e is defined as the Thomson cross-section: $\sigma_e = 8\pi e^4/3m_e^2c^4 = 6.65\cdot10^{-25}$ cm^2. The $ns \to n'l'$ transitions can occur to either s or d angular momentum states. $(gf)_{ik}$ are the weighted oscillator strengths of the hydrogen bound-bound $n_il_i \to n_kl_k$ transitions, ν_{ik} are the corresponding frequencies: $\nu_{ik} = (\epsilon_k - \epsilon_i)/h$. The singularities for $\nu_i = \nu_{im}$ disappear if radiation damping is included; for our applications this effect is irrelevant.

The summation includes all bound states m. If the frequency ν_i of the incident photon lies close to an eigenfrequency, ν_{ir}, of the atom, the scattering cross-section can reasonably well be approximated by

$$\sigma^{(\mathrm{Raman})}_{(ns\to n'l')} \approx \frac{1}{16}\cdot\sigma_e\,\nu_i\nu_f{}^3\left|\mathcal{M}^r_{if}\right|^2. \tag{4}$$

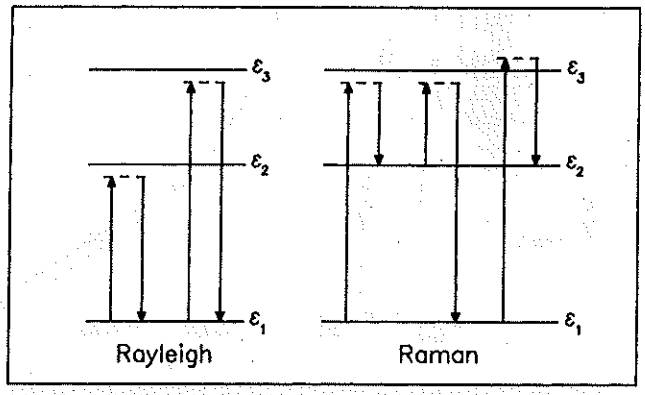

Fig. 1. Schematic picture of Raman and Rayleigh scattering. The dashed lines indicate ϵ_q.